Non-Maxwellian fast particle effects in gyrokinetic GENE simulations

A. Di Siena,[1, a)] T. Görler,[1] H. Doerk,[1] R. Bilato,[1] J. Citrin,[2] T. Johnson,[3] M. Schneider,[4] E. Poli,[1] and JET Contributors[5]

[1)] *Max Planck Institute for Plasma Physics Boltzmannstr 2 85748 Garching Germany*

[2)] *DIFFER Dutch Institute for Fundamental Energy Research De Zaale 20 5612 AJ Eindhoven The Netherlands*

[3)] *VR Association EES KTH Stockholm Sweden*

[4)] *CEA IRFM F13108 Saint Paul Lez Durance France*

[5)] *See the author list of X Litaudon et al 2017 Nucl Fusion 57 102001*

(Dated: 18 April 2018)

Fast ions have recently been found to significantly impact and partially suppress plasma turbulence both in experimental and numerical studies in a number of scenarios. Understanding the underlying physics and identifying the range of their beneficial effect is an essential task for future fusion reactors, where highly energetic ions are generated through fusion reactions and external heating schemes. However, in many of the gyrokinetic codes fast ions are, for simplicity, treated as equivalent-Maxwellian-distributed particle species, although it is well known that to rigorously model highly non-thermalised particles, a non-Maxwellian background distribution function is needed. To study the impact of this assumption, the gyrokinetic code GENE has recently been extended to support arbitrary background distribution functions which might be either analytic, e.g. slowing down and bi-Maxwellian, or obtained from numerical fast ion models. A particular JET plasma with strong fast-ion related turbulence suppression is revised with these new code capabilities both with linear and nonlinear gyrokinetic simulations. It appears that the fast ion stabilization tends to be less strong but still substantial with more realistic distributions, and this improves the quantitative power balance agreement with experiments.

I. INTRODUCTION

A major factor limiting the performance of a fusion reactor is plasma turbulence. It is inevitably driven by steep temperature and density profiles and is one of the main reasons for the energy confinement degradation of nowadays tokamaks. In particular, the ion-temperature-gradient (ITG) instability has been identified as an important driver of microturbulence[1]. Any mechanism able to reduce its development is extremely valuable and can lead to an increase of the energy confinement time. Among the different stabilising mechanisms affecting the ITG microinstability, the presence of fast ions, generated through fusion reactions and/or auxiliary heating, has recently been found to have a significant impact on plasma turbulence. Several studies have indeed shown that fast ions can passively dilute the main ion species[2,3], increase geometric stabilisation, i.e. Shafranov shift stabilization[4] and actively stabilise linear growth rates and nonlinear fluxes through an electromagnetic stabilization related to fast ion suprathermal pressure gradients[5,6]. Furthermore, a wave-particle has recently been identified[7] through which fast particles can affect the main ion microinstability if the fast ion magnetic drift frequency is close to the linear frequency of the mode. This mechanisms can strongly reduce the thermal ITG drive and partially suppress the ion-scale turbulence. Other works have instead tackled the opposite issue, namely to which degree

[a)] Electronic mail: alessandro.di.siena@ipp.mpg.de

turbulence affects the fast ion background distribution function and the associated pressure profiles[8,9]. Thanks to these works significant progress in understanding the fast ions impact on turbulence and vice versa has already been made and a good agreement between numerical and experimental results is often achieved. However, in some of the most prominent studies where fast ions were found to be crucial to obtain realistic heat flux levels, the turbulence suppression appeared to be overestimated and power balance was, e.g., only reached with an increased main ion pressure gradient profile. In these works, an equivalent Maxwellian distribution function was employed for the highly non-thermalised fast ion species. In the contribution at hand, these studies are significantly improved by considering realistic fast ion distribution functions in GENE for the first time. For this purpose, GENE has recently been modified to account for completely arbitrary background distribution functions, which might be either analytic, e.g. slowing down and Bi-Maxwellian, or numerical, e.g. extracted from specialized beam modelling codes like NEMO/SPOT[10] (for the Neutral Beam Injected (NBI) particles) and SELFO[11] or TORIC/SSFPQL[12,13] (for Ion Cyclotron Resonance Heated (ICRH) ions). The associated modifications in the underlying equations and in the source code will be discussed in the following before this new code version will be applied to one of the aforementioned scenarios with substantial fast-ion related turbulence suppression. In detail, this paper is organized as follows. In Sec. II the basic gyrokinetic equations for the full electromagnetic but collisionless case are discussed/derived without any assumptions on the background distribution function. The Vlasov equation, the moments of the distribution function and the Maxwell equations are self-consistently treated on the GENE coordinate grid. The limit of validity of the above derivation is discussed as well. In Sec. III an introduction of a JET L-mode discharge studied in this paper is presented and the non-Maxwellian distribution functions used in the GENE numerical simulations are defined in Sec. III A. A linear and nonlinear analysis with the more realistic distribution functions for the fast ion species is respectively shown in Sec. III B and Sec. III C and finally in Sec. IV general conclusions are drawn.

II. NON-MAXWELLIAN GYROKINETIC EQUATIONS

All the simulations presented in this work have been performed with the gyrokinetic code GENE, which solves numerically the Vlasov-Maxwell system of equations on a five dimensional grid for each time step. GENE can either be operated in the local flux tube approximation[14], in a radially global torus geometry[15] or as a flux-surface code[16]. Furthermore, full electromagnetic effects, realistic collision operators[15] and experimental geometries can be included. In the following section the basic gyrokinetic equations are re-derived in the full electromagnetic case without any assumption on the shape of the background distribution function in a collisionless framework. Collisions will, however, be included in the numerical simulations of Sec. III as they may impact the microinstabilities directly. Invoking a separation of the collisional and turbulent time scales, their effect on the background distributions is neglected for now and Maxwellians are considered in the linearized Landau-Boltzmann collision operator. A more consistent treatment involving a collisional operator for non-thermalized distributions will be studied in a future publication. This general derivation allows a very flexible treatment of non-thermalised fast ion species, able to capture asymmetries and anisotropies of the background distribution function which might arise from the different heating schemes of a tokamak reactor.

A. Vlasov equation

The Vlasov equation determines the time evolution of the distribution function of each plasma species and in the gyro-center coordinate system $(\mathbf{X}, v_{\shortparallel}, \mu)$ can be written as

follows[17]

$$\frac{\partial F}{\partial t}+\frac{d\mathbf{X}}{dt}\cdot\nabla F+\frac{dv_{\shortparallel}}{dt}\frac{\partial F}{\partial v_{\shortparallel}}+\frac{d\mu}{dt}\frac{\partial F}{\partial \mu}=0. \quad (1)$$

Here, $\mathbf{X}$ represents the centre of gyration, $v_{\shortparallel}$ the velocity along the magnetic field line and μ the magnetic moment. Expliciting the time derivatives of the coordinates[15], Eq. 1 can be written as

$$\begin{aligned}&\frac{\partial F}{\partial t}+\left[v_{\shortparallel}\hat{b}_0+(\vec{v}_E+\vec{v}_{\nabla B}+\vec{v}_c)\right]\\&\cdot\left\{\vec{\nabla}F-\left[q\vec{\nabla}\bar{\phi}_1+\frac{q}{c}\hat{b}_0\dot{\bar{A}}_{1,\shortparallel}\right.\right.\\&\left.\left.+\mu\vec{\nabla}\left(B_0+\bar{B}_{1,\shortparallel}\right)\right]\frac{1}{mv_{\shortparallel}}\frac{\partial F}{\partial v_{\shortparallel}}\right\}=0.\end{aligned} \quad (2)$$

Here, the curvature, $E\times B_0$ and ∇B_0 drift velocities have been defined as $\vec{v}_c=\frac{v_{\shortparallel}^2}{\Omega}\left(\vec{\nabla}\times\hat{b}_0\right)_{\perp}$, $\vec{v}_E=\frac{c}{B_0^2}\left(\vec{B}_0\times\vec{\nabla}\bar{\xi}_1\right)$ and $\vec{v}_{\nabla B_0}=\frac{\mu}{qB_0^2}\left(\vec{B}_0\times\vec{\nabla}B_0\right)$. Furthermore, $\bar{\xi}_1$ denotes the modified potential $\bar{\xi}_1=\bar{\phi}_1-\frac{v_{\shortparallel}}{c}\bar{A}_{1,\shortparallel}+\frac{\mu}{q}\bar{B}_{1,\shortparallel}$; $\Omega=\frac{qB_0}{mc}$ the gyrofrequency and $\hat{b}_0=\frac{\vec{B}_0}{B_0}$ the unit vector along the magnetic field. The overbar denotes gyroaveraged quantities, which in the local code approximation reduce to the mere multiplication of Bessel functions, i.e. $\bar{\phi}_1=J_0(\lambda)\phi_1$, $\bar{A}_{1,\shortparallel}=J_0(\lambda)A_{1,\shortparallel}$ and $\bar{B}_{1,\shortparallel}=I_1(\lambda)B_{1,\shortparallel}$, where $I_1(\lambda)=\frac{2}{\lambda}J_1(\lambda)$ and $\lambda=\frac{k_{\perp}}{\Omega}(\frac{2B_0\mu}{m})^{1/2}$. Furthermore, B_0 denotes the background magnetic field, E the perturbed electric field defined as $\vec{E}=\vec{\nabla}\bar{\xi}_1$, q and m, respectively, the charge and the mass of the considered species, c the speed of light and $k_{\perp}$ the perpendicular wavenumber.

An often employed approach in gyrokinetics is the splitting of the distribution function of each species into a background component and in a small fluctuating part, i.e. $F=F_0+F_1$ (so-called δf). While many derivations like the previous one for GENE rely on local Maxwellian distributions, here we relax such assumption on F_0. The gyrokinetic δf ordering, i.e. $n_1/n_0\sim\epsilon\ll 1$, allows us to greatly simplify the numerical solution of Eq. 2. It is indeed possible to separate the time scale of variation of the background from the one of the fluctuating quantities through the expansion parameter ϵ. The zeroth order term of the Vlasov equation, which reads as

$$\frac{\partial F_0}{\partial t}=\hat{b}_0\cdot\left(v_{\shortparallel}\vec{\nabla}F_0-\frac{\mu}{m}\vec{\nabla}B_0\frac{\partial F_0}{\partial v_{\shortparallel}}\right) \quad (3)$$

is exactly zero for local Maxwellian background (defined in Eq. 25). The mirror force term - right hand side of Eq. 3 - does not modify F_0. The zeroth order quantities can hence be considered time independent on the turbulent time scale. For the case of an arbitrary background distribution function, Eq. 3 is not necessarily zero and the degree of violation of Eq. 3 must be studied case by case. In section III A an accurate analysis of Eq. 3 is done for the numerical distribution functions employed in this paper. The turbulent evolution of the system is determined by the first order term of Eq. 2. It is convenient, at this point, to introduce a field aligned coordinate system, defined through the metric coefficients $g^{ij}=\nabla u^i\cdot\nabla u^j$, with $u^i=(x,y,z)$, x radial direction, y binormal direction and direction parallel to the magnetic field z. The strong anisotropy of plasma turbulence with respect to the magnetic field, i.e. $k_{\perp}/k_{\shortparallel}<<1$, enables further simplification of the first order term in Eq. 2, which becomes

$$\begin{aligned}&\frac{\partial g_1}{\partial t}+\frac{C}{JB_0}\left\{v_{\shortparallel}\partial_z F_1-\left(\frac{q}{m}\partial_z\bar{\phi}_1\frac{\partial F_0}{\partial v_{\shortparallel}}\right.\right.\\&\left.\left.+\frac{\mu}{m}\partial_z B_0\frac{\partial F_1}{\partial v_{\shortparallel}}+\frac{\mu}{m}\partial_z\bar{B}_{1,\shortparallel}\frac{\partial F_0}{\partial v_{\shortparallel}}\right)\right\}\\&+\frac{c}{C}\left(\frac{g^{1i}g^{2j}-g^{2i}g^{1j}}{\gamma_1}\right)\left\{\left[\partial_i\bar{\xi}_1+\frac{\mu}{q}\partial_i B_0\right.\right.\\&\left.+\frac{v_{\shortparallel}^2 m}{q}\left(\frac{\partial_i B_0}{B_0}+\frac{\beta_p}{2}\frac{\partial_i p_0}{p_0}\right)\right]\cdot\left[\partial_j F_0+\partial_j F_1\right.\\&\left.\left.-\left(q\partial_j\bar{\phi}_1+\mu\partial_j B_0+\mu\partial_j\bar{B}_{1,\shortparallel}\right)\frac{1}{mv_{\shortparallel}}\frac{\partial F_0}{\partial v_{\shortparallel}}\right]\right\}=0.\end{aligned} \quad (4)$$

Here, a modified distribution function $g_1=F_1-\frac{q}{mc}\bar{A}_{1,\shortparallel}\frac{\partial F_0}{\partial v_{\shortparallel}}$ has been introduced and the following geometrical coefficients have been defined $\gamma_1=g^{11}g^{22}-g^{21}g^{12}$, $C=B_0/\gamma_1^{1/2}$ and

$J = B_0 \cdot \nabla z/C$. Eq. 4 is solved in dimensionless units. To aim, all the physical quantities have been split into a dimensionless value and a dimensional reference part. The reference values used for normalizing Eq. 4 are the elementary electron charge e, the main ion mass m_i and temperature T_i, a reference magnetic field $B_{\rm ref}$ and a macroscopic length $L_{\rm ref}$. The normalized Vlasov equation for a completely general background distribution function can be written as follows

$$\begin{aligned}\frac{\partial g_1}{\partial t} = &-\frac{C}{JB_0} v_{th} v_{\shortparallel} \left[\partial_z F_1 - \frac{q}{2T_0 v_{\shortparallel}} \partial_z \phi_1 \frac{\partial F_0}{\partial v_{\shortparallel}} - \frac{\mu}{2v_{\shortparallel}} \partial_z B_{1,\shortparallel} \frac{\partial F_0}{\partial v_{\shortparallel}}\right] + \frac{C}{JB_0} v_{th} \frac{\mu}{2} \partial_z B_0 \frac{\partial F_1}{\partial v_{\shortparallel}} \\ &+ \frac{T_0}{q}\left(\frac{\mu B_0 + 2v_{\shortparallel}^2}{B_0}\right)\mathcal{K}_x \hat{\partial}_x F_0 - \frac{T_0}{q}\left[\left(\frac{\mu B_0 + 2v_{\shortparallel}^2}{B_0}\right)\mathcal{K}_y - \frac{1}{C}\frac{v_{\shortparallel}^2 \beta_{ref}}{B_0^2}\omega_p\right]\partial_y g_1 \\ &+ \left[\frac{1}{2v_{\shortparallel}}\frac{\partial F_0}{\partial v_{\shortparallel}}\left(\frac{\mu B_0 + 2v_{\shortparallel}^2}{B_0}\right)\mathcal{K}_y - \frac{1}{C}\frac{v_{\shortparallel}^2 \beta_{ref}}{B_0^2}\omega_p \frac{1}{2v_{\shortparallel}}\frac{\partial F_0}{\partial v_{\shortparallel}} - \frac{1}{C}\hat{\partial}_x F_0\right]\partial_y \xi_1 \\ &- \frac{T_0}{q}\left(\frac{\mu B_0 + 2v_{\shortparallel}^2}{B_0}\right)\mathcal{K}_x \partial_x g_1 + \frac{1}{2v_{\shortparallel}}\frac{\partial F_0}{\partial v_{\shortparallel}}\left(\frac{\mu B_0 + 2v_{\shortparallel}^2}{B_0}\right)\mathcal{K}_x \partial_x \xi_1 - \frac{1}{C}\left[\partial_x \xi_1 \partial_y g_1 - \partial_y \xi_1 \partial_x g_1\right]\end{aligned} \tag{5}$$

where the following geometrical coefficients $\mathcal{K}_x = -\frac{1}{C}\left(\partial_y B_0 - \frac{\gamma_3}{\gamma_1}\partial_z B_0\right)$, $\mathcal{K}_y = \frac{1}{C}\left(\partial_x B_0 - \frac{\gamma_3}{\gamma_1}\partial_z B_0\right)$; the normalized radial derivative $\hat{\partial}_x = -(\partial_x - \frac{\mu}{2v_{\shortparallel}}\partial_x B_0 \frac{\partial}{\partial v_{\shortparallel}})$; the normalized background pressure gradient $\omega_p = -L_{\rm ref}\frac{\partial_x p_0}{n_{\rm ref} T_{\rm ref}}$ and the reference thermal to magnetic pressure ratio $\beta_{\rm ref} = \frac{8\pi n_{\rm ref} T_{\rm ref}}{B_{\rm ref}^2}$ have been defined. If the equilibrium distribution function F_0 is a local Maxwellian, Eq. 5 reduces to the gyrokinetic equation known in literature[15,17].

B. Velocity space moments

In order to treat self-consistently the Vlasov-Maxwell system of coupled equations, the fluctuating component of the fields must be evaluated from the perturbed distribution function of each plasma species at every time step. Therefore, a general description of the various F_1 velocity space moments appearing in the field equations is presented without making any assumptions on the background distribution function. The general a-th moment in $v_{\shortparallel}$ and b-th in μ (or, more precisely, in $v_\perp$) in the guiding centre coordinate system $(\mathbf{X}, \theta, v_{\shortparallel}, \mu)$ is defined as follows

$$M_{a,b}(\mathbf{x}) = 2^{b/2}\left(\frac{B_0}{m}\right)^{b/2+1}\int \delta(\mathbf{X} + \mathbf{r} - \mathbf{x})\, f_1^{gc}(\mathbf{X}, \theta, v_{\shortparallel}, \mu)\, v_{\shortparallel}^a \mu^{b/2} d^3X dv_{\shortparallel} d\mu d\theta. \tag{6}$$

Here, $f_1^{gc}(\mathbf{X}, \theta, v_{\shortparallel}, \mu)$ is the perturbed distribution function in the guiding centre coordinate system and δ is the Dirac-delta function. The space transformation used to link the particle coordinates to the guiding centre is $\mathbf{x} = \mathbf{X} + \mathbf{r}(\mathbf{X}, \mu, \theta)$, where $\mathbf{r}$ denotes the gyroradius

vector. As the time evolution of the perturbed distribution function (Eq. 5) is performed in the gyro centre coordinate system it is necessary to define an operator T^* which transforms F_1 from the gyro centre to the guiding centre coordinate system. Up to the first order in the gyrokinetic expansion[17,18] this so-called pull-back operator is defined as follows

$$f_1^{gc}\left(\mathbf{X},\theta,v_{\shortparallel},\mu\right)=T^*F_1\left(\mathbf{X},v_{\shortparallel},\mu\right) \tag{7}$$

$$\begin{aligned}=F_1+\frac{1}{B_0}\Bigg\{\left[\Omega\frac{\partial F_0}{\partial v_{\shortparallel}}-\frac{q}{c}v_{\shortparallel}\frac{\partial F_0}{\partial\mu}\right]\left(A_{1,\shortparallel}\left(\mathbf{X}+\mathbf{r}\right)\right.\\ \left.-\bar{A}_{1,\shortparallel}\left(\mathbf{X}\right)\right)\\ +\left[q\left(\phi_1\left(\mathbf{X}+\mathbf{r}\right)-\bar{\phi}_1\left(\mathbf{X}\right)\right)-\mu\bar{B}_{1,\shortparallel}\right]\frac{\partial F_0}{\partial\mu}\Bigg\}.\end{aligned} \tag{8}$$

By performing the integrals over θ and $\mathbf{X}$ and using the previously defined operator, the generic moment of the gyro centre distribution function reduces to

$$\begin{aligned}M_{a,b}\left(\mathbf{x}\right)=\pi\left(\frac{2B_0}{m}\right)^{b/2+1}\int\Bigg\{\left\langle F_1\left(\mathbf{x}-\mathbf{r}\right)\right\rangle+\left(\frac{\Omega}{B_0}\frac{\partial F_0}{\partial v_{\shortparallel}}-\frac{q}{cB_0}v_{\shortparallel}\frac{\partial F_0}{\partial\mu}\right)\left(A_{1,\shortparallel}\left(\mathbf{x}\right)-\left\langle\bar{A}_{1,\shortparallel}\left(\mathbf{x}-\vec{r}\right)\right\rangle\right)\\ +\left[\frac{q}{B_0}\left(\phi_1\left(\mathbf{x}\right)-\left\langle\bar{\phi}_1\left(\mathbf{x}-\mathbf{r}\right)\right\rangle\right)-\frac{\mu}{B_0}\left\langle\bar{B}_{1,\shortparallel}\left(\mathbf{x}-\mathbf{r}\right)\right\rangle\right]\frac{\partial F_0}{\partial\mu}\Bigg\}v_{\shortparallel}^a\mu^{b/2}dv_{\shortparallel}d\mu,\end{aligned} \tag{9}$$

where $\langle ...\rangle=\frac{1}{2\pi}\int ...d\theta$. In the specific case of a Maxwellian background, Eq. 9 can be greatly simplified, i.e. the term that multiplies the vector potential is exactly zero. As it will be shown in the next section, the latter simplification leads to a decoupling between the Poisson and $B_{1,\shortparallel}$ equations and the parallel component of the Ampere's law. This is not necessarily the case for non-Maxwellian distribution functions.

C. Field equations

The Poisson equation and the Ampere's law for both the parallel and perpendicular component of the electromagnetic potential can be written in terms of the $M_{0,0}$, $M_{1,0}$ and $M_{0,1}$ moments of the perturbed distribution function F_1 as follows

$$\begin{aligned}\nabla^2_{\perp}\phi_1\left(\mathbf{x}\right)&=-4\pi\sum_j q_j n_{1,j}\left(\mathbf{x}\right)\\ &=-4\pi\sum_j q_j M_{0,0,j}\left(\mathbf{x}\right),\end{aligned} \tag{10}$$

$$\begin{aligned}-\nabla^2_{\perp}A_{1,\shortparallel}\left(\mathbf{x}\right)&=\frac{4\pi}{c}\sum_j j_{\shortparallel,1,j}\left(\mathbf{x}\right)\\ &=\frac{4\pi}{c}\sum_j q_j M_{1,0,j}\left(\mathbf{x}\right),\end{aligned} \tag{11}$$

$$\begin{aligned}&\hat{e}_1\partial_y B_{1,\shortparallel}\left(\mathbf{x}\right)+\hat{e}_2\partial_x B_{1,\shortparallel}\left(\mathbf{x}\right)\\ &=\frac{4\pi}{c}\sum_j\vec{j}_{1,\perp,j}\left(\mathbf{x}\right)\\ &=\frac{4\pi}{c}\sum_j q_j\hat{c}(\theta)M_{0,1,j}\left(\mathbf{x}\right).\end{aligned} \tag{12}$$

The field equations have been written in the particle coordinate system $\left(\hat{e}_1, \hat{e}_2, \hat{b}_0\right)$, where $\hat{c}(\theta)$ is the unit vector in the perpendicular plane, $\hat{c}(\theta) = -\sin\theta\hat{e}_1 + \cos\theta\hat{e}_2$. From Eq. 9 it is possible to reformulate the field equations in terms of the perturbed distribution function F_1 as it is done, in dimensionless units, in Eq. 13, 14, 15. In the following equations the sum over all species is omitted for better readability.

$$P\phi_1(\mathbf{x}) + \mathcal{F}A_{1,\shortparallel}(\mathbf{x}) + \mathcal{T}B_{1,\shortparallel}(\mathbf{x}) = q\pi n_0 B_0 \int J_0 g_1(\mathbf{x})\, dv_\shortparallel d\mu \tag{13}$$

$$\mathcal{L}\phi_1(\mathbf{x}) + \mathcal{H}A_{1,\shortparallel}(\mathbf{x}) + \mathcal{K}B_{1,\shortparallel}(\mathbf{x}) = qn_0\pi\beta_{ref}\frac{B_0 v_{th}}{2}\int v_\shortparallel J_0 g_1(\mathbf{x})\, dv_\shortparallel d\mu \tag{14}$$

$$\mathcal{R}\phi_1(\mathbf{x}) + \mathcal{W}A_{1,\shortparallel}(\mathbf{x}) + \mathcal{Q}B_{1,\shortparallel}(\mathbf{x}) = B_0^{\frac{3}{2}}\frac{q\pi n_0 v_{th}}{2k_\perp}\beta_{ref}\int \sqrt{\mu} J_1 g_1(\mathbf{x})\, dv_\shortparallel d\mu \tag{15}$$

The following operators have been defined

$$P = k_\perp^2\lambda_{De}^2 - \frac{\pi q^2 n_0}{T_0}\int\left(1 - J_0^2\right)\frac{\partial F_0}{\partial\mu}dv_\shortparallel d\mu \tag{16}$$

$$\mathcal{F} = \frac{2\pi q^2 n_0}{m v_{th}}\int\left[\left(1 - J_0^2\right)v_\shortparallel\frac{\partial F_0}{\partial\mu} - \frac{B_0}{2}\frac{\partial F_0}{\partial v_\shortparallel}\right]dv_\shortparallel d\mu \tag{17}$$

$$\mathcal{T} = \pi q n_0\int\mu J_0 I_1\frac{\partial F_0}{\partial\mu}dv_\shortparallel d\mu \tag{18}$$

$$\mathcal{H} = k_\perp^2 - \frac{q^2 n_0\pi\beta_{ref}}{m}\int\left[B_0\frac{v_\shortparallel}{2}\frac{\partial F_0}{\partial v_\shortparallel} - v_\shortparallel^2\frac{\partial F_0}{\partial\mu}\left(1 - J_0^2\right)\right]dv_\shortparallel d\mu \tag{19}$$

$$\mathcal{L} = \frac{q^2 n_0\pi\beta_{ref}}{m v_{th}}\int\frac{\partial F_0}{\partial\mu}\left(1 - J_0^2\right)v_\shortparallel dv_\shortparallel d\mu \tag{20}$$

$$\mathcal{K} = \frac{v_{th}}{2}\int J_0 I_1 v_\shortparallel\mu\frac{\partial F_0}{\partial\mu}dv_\shortparallel d\mu \tag{21}$$

$$\mathcal{Q} = -1 + \frac{\pi q^2 n_0 B_0}{m k_\perp^2}\beta_{ref}\int\mu\frac{\partial F_0}{\partial\mu}J_1^2 dv_\shortparallel d\mu \tag{22}$$

$$\mathcal{W} = -B_0^{\frac{1}{2}}\frac{q^2 n_0}{m k_\perp}\beta_{ref}\int\sqrt{\mu}v_\shortparallel J_1 J_0\frac{\partial F_0}{\partial\mu}dv_\shortparallel d\mu \tag{23}$$

$$\mathcal{R} = B_0^{\frac{1}{2}}\frac{\pi q^2 n_0}{m k_\perp v_{th}}\beta_{ref}\int\sqrt{\mu}\frac{\partial F_0}{\partial\mu}J_1 J_0 dv_\shortparallel d\mu \tag{24}$$

where $\lambda_{De} = \sqrt{\frac{B_{\mathrm{ref}}^2}{4\pi c^2 n_{\mathrm{ref}} m_{\mathrm{ref}}}}$ is the normalized Debye length. For a completely general background distribution function each component of the fields is coupled to the others. This system decouples for the $A_{1,\shortparallel}$ component if a Maxwellian distribution functions is chosen, since $\mathcal{F} = \mathcal{W} = \mathcal{L} = \mathcal{K} = 0$.

III. APPLICATION OF REALISTIC FAST PARTICLE BACKGROUND DISTRIBUTIONS

Taking advantage of these new capabilities of the gyrokinetic code GENE, experimental discharges associated to significant fast ion stabilisation can now be studied with the more realistic modelling tools for the energetic ion population introduced in Sec. II. The newly implemented terms have been benchmarked with the gyrokinetic codes GKW and GS2 for simplified geometry and in the electrostatic limit in Ref. 19 and in the work at hand a realistic scenario is extensively studied. The JET C-wall L-mode plasma 73224 has been selected and re-analysed with the more realistic non-Maxwellian distribution functions. The experiment was performed with vacuum toroidal magnetic field $B_T \approx 3.3$T, plasma current $Ip \approx 2$MA and with

$q_{95} \approx 6$. The heating power consists of 3.5MW of ICRH in $(3He)D$ minority scheme and of 1.5MW of NBI. Furthermore, the ICRH power was deposited on-axis. The plasma was composed of bulk thermal Deuterium, electrons and Carbon impurities and of fast NBI Deuterium and ICRH ^{3}He. An accurate description of this discharge can be found in Ref. 20–22. Experimental geometry, collisions (Landau-Boltzmann operator), electromagnetic fluctuations and kinetic electrons are included. The magnetic geometry and the nominal plasma parameters are summarised in table I and the radial thermal density and temperature profiles, reconstructed by CRONOS simulations, are shown in Fig. 1. The analysis of this discharge is performed in the local flux tube approximation at a radial position of $\rho_{\text{tor}} = 0.33$, i.e. where a significant fast ion turbulence suppression is observed. The local approach is justified by low values of the ion Larmor radius normalized to the tokamak minor radius, i.e. ρ_i/a, with $\rho_i = (T_i/m_i)^{1/2}/\Omega$, namely $\rho^* = 1/450$ for thermal ions and $\rho^*_{fast,D} = 1/150$; $\rho^*_{^3He} = 1/200$, respectively, for fast deuterium and helium.

A. Equilibrium distribution functions

As mentioned in section II, a δf approach is employed for solving the gyrokinetic system of equations where the distribution function of each species is split into a time independent background component and a small fluctuating part. For all the thermal species, the background F_0 is assumed to be the local Maxwellian distribution function as defined as follows

$$F_{0,M} = \frac{n_0}{\pi^{3/2} v_{th}^3} \exp\left(\frac{-m v_{\shortparallel}^2/2 - \mu B_0}{T_0}\right). \quad (25)$$

Here, m is the particle mass, T_0 the equilibrium temperature, n_0 the particle density, $v_{th} = (2T_0/m)^{1/2}$ the thermal velocity and B_0 the equilibrium magnetic field. For the case of energetic ions the more flexible F_0 setup presented in Sec. II has been implemented in the code. GENE is now able to support a large variety of different background distribution functions which can be either analytical or numerical. Exploiting this feature, it is possible to capture individual asymmetries and anisotropies in the distribution function arising from the different heating schemes, e.g. ICRH and NBI. When the distribution function of the fast ion species is calculates with Monte Carlo codes, such as SPOT/NEMO and SELFO, irregularities of the distribution functions may appear. Here they have been reduced by the application of 3D Gaussian filters, also known as Weierstrass transformation. In more detail, the smoothed distribution functions were the result of a convolution integral, in each dimension, with a Gaussian kernel, which preserves boundaries but reduces the high-frequency components. For the case of NBI fast Deuterium a numerical distribution function has been extracted from SPOT/NEMO simulations with 4191 test particles and has been interpolated on the GENE coordinate grid. In Fig. 2a) the numerical SPOT/NEMO distribution function is shown on the GENE $v_{\shortparallel} - \mu$ grid. A velocity space structure similar to a slowing down distribution can be identified with a cut-off velocity $v_{\shortparallel,c} \sim 1.5$. Furthermore, a strong velocity anisotropy between co-passing and counter-passing fast particles is observed. In the next paragraph a linear analysis is performed studying the impact of the different backgrounds on the more unstable growth rates and frequencies. Regarding the NBI fast deuterium, the results obtained with the SPOT/NEMO distribution function are compared to the ones obtained with the analytic slowing-down function derived in Ref. 24 and, e.g., used in Ref. 25 for modelling fusion born alpha particles. The latter is a solution of the Fokker-Planck equation with an isotropic delta-function particle source and is defined as follows

$$F_{0,s} = \frac{3n_0}{4\pi \log\left(1 + \frac{v_\alpha^3}{v_c^3}\right)\left[v_c^3 + v^3\right]} \Theta\left(v_\alpha - v\right). \quad (26)$$

Here, the birth velocity is defined through the birth energy E_α in the following way $v_\alpha = (2E_\alpha/m_\alpha)^{1/2}$, while

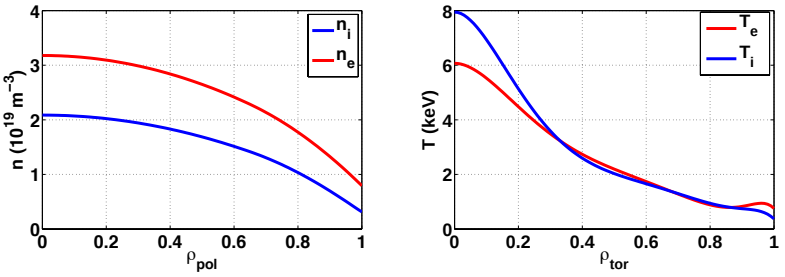

FIG. 1. Radial profiles of main ions (blue line) and electron (red line) a) temperature and b) density for the discharge 73224.

TABLE I. Parameters at $\rho_{\rm tor} = 0.33$ for the JET L-mode discharge 73224 according to Ref. 22 and 23. T represents the temperature normalized to the electron one, $R/L_{T,n}$ the normalized logarithmic temperature and density gradients and ν^* the electron-ion collision frequency normalized to the trapped electron bounce frequency.

R	$\hat{s}$	q	T_e/T_i	R/L_{T_i}	R/L_{T_e}	R/L_{n_e}	ν^*
3.1	0.5	1.7	1.0	9.3	6.8	1.3	0.038
n_{fD}	$n_{^3He}$	T_{fD}	$T_{^3He}$	$R/L_{T_{fD}}$	$R/L_{T_{^3He}}$	R/L_{nfD}	$R/L_{n_{^3He}}$
0.06	0.07	9.8	6.9	3.2	23.1	14.8	1.6

$v_c = v_{th,e}\left(\frac{3\sqrt{\pi}m_e}{4}\sum_{\text{main ions}}\frac{n_i z_i^2}{n_e m_i}\right)^{1/3}$ represents the crossover velocity. Furthermore, Θ is the Heaviside step function.

For the case of the ICRH ^{3}He, numerical distribution functions extracted from TORIC/SSFPQL and SELFO are used both in the linear and turbulence analysis presented in this work. Interface routines between these different codes and GENE have been implemented. The SPOT/NEMO and SELFO numerical distribution functions, here employed, had already been used in Ref. 6 to calculate the fast ion profiles for the equivalent Maxwellian distribution function respectively for the NBI and ICRH-driven fast ions. In Fig. 2b) the phase space structure of ^{3}He distribution functions extracted from TORIC/SSFPQL is shown on the GENE coordinate grid. No significant difference with the SELFO background is observed. Similar to the NBI fast Deuterium which has been approximated by a slowing down distribution (Eq. 26), a first order analytical approximation is employed for the ICRH generated ^3He. Namely a bi-Maxwellian distribution function

$$F_{0,aM} = \frac{n_0}{\pi^{3/2} v_{th,\shortparallel} v_{th,\perp}^2}\exp(-v_\shortparallel^2/v_{th,\shortparallel}^2 - \frac{\mu B_0}{T_\perp}), \tag{27}$$

is used in order to account for the velocity space anisotropies arising from the ICRH heating. Here, $T_\shortparallel$ and $T_\perp$ are respectively the parallel and perpendicular temperatures. The $T_\perp/T_\shortparallel = 2.2$ and $L_{T_\shortparallel}/L_{T_\perp} = 3$ anisotropies have been extracted from SELFO simulations and are consistent with the ones evaluated with TORIC/SSFPQL. Furthermore, the fast particle temperatures have been defined as the second order moment of the numerical distribution functions[25,26], i.e. NEMO/SPOT for the NBI fast deuterium and TORIC/SSFPQL and SELFO for the ICRH ^{3}He, namely

$$T = \frac{\int v^2 F_{0,\text{numerical}} d^3v}{\int F_{0,\text{numerical}} d^3v}. \tag{28}$$

One of the major constraints on the analytic

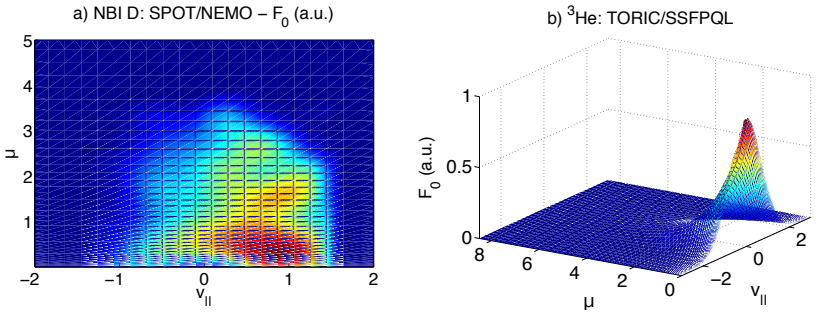

FIG. 2. θ-integrated a) SPOT/NEMO and b) TORIC/SSFPQL numerical distribution functions on the $(v_{\shortparallel}, \mu)$ velocity grid, respectively for NBI fast Deuterium and ICRH ^3He.

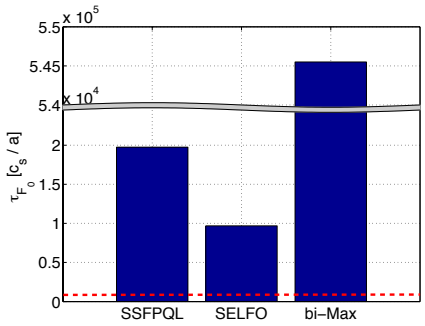

FIG. 3. Comparison between the time scale of variation τ_{F_0} of the backgrounds employed in the turbulence analysis of Sec. III C and the average time of GENE nonlinear simulations - red dotted line - in units of c_s/a.

derivation of Sec. II is set by Eq. 3. The time scale of background distribution variations $\tau_{F_0} = F_0/(\partial F_0/\partial t)$ described by the zeroth order Vlasov equation should always be well separated from the turbulent time scale. While this can be easily shown for local Maxwellians and slowing down backgrounds, other distribution functions like the numerical and bi-Maxwellian ones require a more detailed study of Eq. 3. However, it is worth specifying that the F_0 provided by heating codes is not the solution of the simple Eq. 3, where the equilibrium is established only by the mirror force. On the contrary, the numerical backgrounds are the steady-state solution of the kinetic equation which includes also collisions and sources/sinks. These distribution functions represent the equilibrium between the fast ion excitation (or birth) process and the collisions, and hence they are not expected to be modified on turbulence timescales. With the assumption that the time scale characteristic of the mirror force, τ_{F_0}, is much faster than the collisional one, it is possible to reduce the study of evolution of the numerical background by solving Eq. 3. Corresponding results are shown in Fig. 3 and demonstrate that the average time - normalized to c_s/a - required in the GENE nonlinear simulations to reach a saturated turbulence state is several order of magnitudes smaller than τ_{F_0}. Therefore, if F_0 is perturbed, it reaches a new equilibrium on a much longer time scale than the one turbulence need to reach saturation. The background distributions can thus be considered constant in time.

B. Linear growth rate analysis

This section adresses the impact of the more realistic distribution functions on the ITG microturbulence. Although a true comparison with experiments can only be made with fully nonlinear simulations (see next session), it is still possible to extract valuable information

about the expected nonlinear sensitivity of the ITG dominated physics on the different fast ion backgrounds from the single mode analysis in the framework of the quasilinear theory. Previous studies shown in Ref. 19 are here extended by including growth rates and frequencies obtained with the fast-ion numerical distribution functions. To resolve the fine velocity-space structure of the numerical backgrounds, 68 points have been used for both the $v_{\shortparallel}$ and the μ GENE grids with simulations box sizes of respectively $(9, 3)$ in normalized units. For the analytic backgrounds, 32 $v_{\shortparallel}$ points and 48 μ points have been found to be sufficient. A first linear analysis is performed on the NBI fast Deuterium. In Fig. 4 the GENE growth rates and frequencies are shown for different $k_y\rho_i$ values or equivalently for different toroidal mode numbers n. All the plasma species have been modelled with a local Maxwellian with the exception of the NBI fast Deuterium which, instead, has been modelled with the different analytical (slowing down) and numerical (NEMO/SPOT) distributions introduced in the previous paragraph. The growth rates and frequencies have been normalized to c_s/a with $c_s = (T_e/m_i)^{1/2}$. A low sensitivity to the change of the fast Deuterium distribution function is observed. The velocity space anisotropies, well captured only from the numerical NEMO/SPOT distribution, do not significantly modify the linear results and only a relative difference of a few percent, i.e. $\lesssim 10\%$, is observed. The slowing down distribution function seems to be a better approximation for the numerical NEMO/SPOT results than the local Maxwellian. Furthermore, for this specific choice of fast Deuterium parameters, lower growth rates are found with the more realistic distributions. A similar analysis can be performed for the ICRF-heated ^{3}He. All the thermal plasma species have been modelled with a local Maxwellian while the NBI fast Deuterium background is either described by a Maxwellian or a slowing down, which has been found to be the best analytical approximation to the NEMO/SPOT distribution. In Fig. 5, linear growth rates and frequencies are displayed for different ^{3}He backgrounds. In contrast to the previous results for fast deuterium, it is shown that the ICRH ^{3}He has a significant impact on the linear ITG physics and differences of $\sim 50\%$ are observed. A change in the background distribution and its radial derivative leads to a consequent change of the resonant ITG-fast ion stabilisation, which is particularly relevant in this discharge[7]. For nominal parameters, the resonance ITG stabilising mechanism is predicted to be much more effective for the ICRF-heated ^{3}He than for the NBI fast Deuterium, which might explain the lack of sensitivity of the fast Deuterium results to the different backgrounds. Moreover, with the more realistic ^{3}He distribution functions a weakening of the still substantial fast ion stabilisation is observed. Fig. 4 also contains simulation results without fast ion effects for reference. These have been obtained by removing all kinetic effects and by consistently modifying the overall geometrical pressure gradient. The dominance of the kinetic effects on setting the difference between "with" and "without" fast ions has been well established from dedicated scans involving turning on and off the various physics effects (modification of drift frequency, Shafranov shift, kinetic effects) in previous work on similar discharges[27]. These results are consistent with experimental observations[6] and predict an overestimation of equivalent-Maxwellian fast-ion stabilisation for the nominal plasma parameters. According to quasilinear models an increase in the linear growth rates might lead to a relative increase of the nonlinear fluxes, greatly improving the agreement with experiments. Furthermore, an excellent agreement between the linear results obtained with TORIC/SSFPQL and SELFO is shown in Fig 5. The bi-Maxwellian has been found to be a good analytical approximation for the growth rate analysis to the numerical distributions in the low $k_y\rho_i \sim 0.1 - 0.3$ wave number range, where most of the transport typically originates in nonlinear ITG simulations.

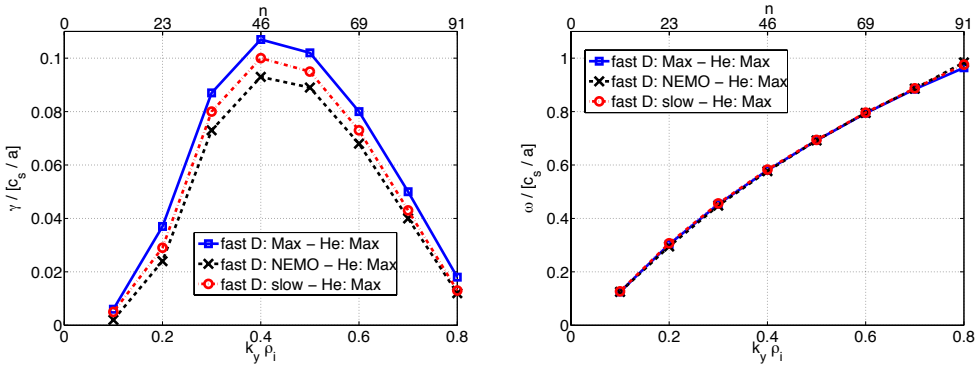

FIG. 4. GENE calculation of the linear growth rates (a) and frequency (b) for different $k_y\rho_i$ and toroidal mode numbers n for different distribution functions for the fast Deuterium.

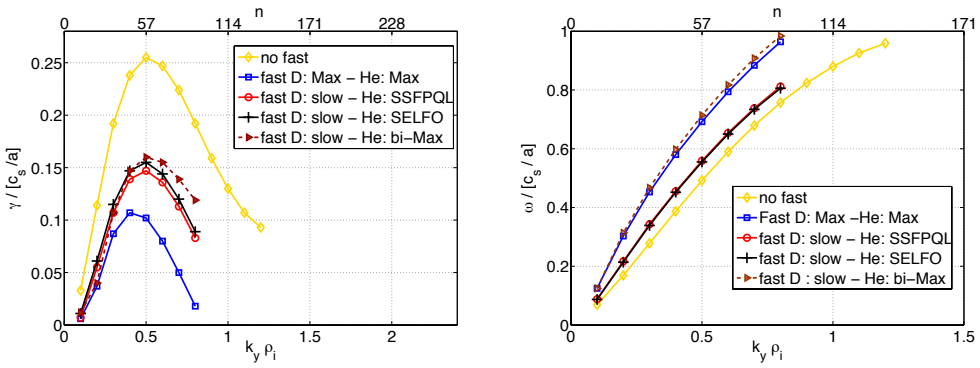

FIG. 5. GENE calculation of the linear growth rates (a) and frequency (b) for different $k_y\rho_i$ and toroidal mode numbers n for different distribution functions for the fast ^{3}He.

C. Turbulence analysis

The impact of more realistic fast-ion distribution functions on the turbulent transport of the low-beta JET discharge 73224 is studied with GENE nonlinear simulations. The physical parameters are the same as in table I. The radial box size is $175\rho_i$ and the minimum finite $k_y\rho_i$ is set to 0.05. We used 192 grid points in radial direction, 48 modes in the binormal direction and 32 points along the field line. As for the linear simulations, a high velocity space resolution is required to resolve the fine velocity structure of the non-Maxwellian distribution functions. In velocity space, 68 points and 68 equidistant symmetric grid points have been used for the numerical distributions and 48, 32 for the analytical backgrounds for resolving respectively the μ and the $v_{\shortparallel}$ space with a $(\mu, v_{\shortparallel})$ box size of respectively $(9, 3)$ in normalized units. The first nonlinear analysis presented in this paper aims at studying the main ion and electron fluxes. In a previous publication[6], it has been shown that a reasonable agreement between the numerical and the experimental values - extracted from CRONOS[28] interpretative simulations - could only be achieved by including equivalent Maxwellian fast ions in the nu-

merical simulations. However, the experimental fluxes were matched only by an increase of the main ion temperature gradient of $\sim$ 20% which may be due to an overestimation of the fast particle stabilizing effects at the nominal plasma parameters. In Fig. 6 a comparison between the nonlinear results obtained with the more realistic fast ion distribution functions and their analytic approximations is shown for values of the main ion temperature gradients inside the experimental error bars. In order to keep the same notation as in Ref. 20–22, the particle and heat fluxes are normalised, respectively, to $\Gamma_{gB} = v_{th,i}\rho_i^2 n_i/R_0^2$ and $Q_{gB} = v_{th,i}\rho_i^2 n_i T_i/R_0^2$. Furthermore, the NBI fast deuterium has been modelled either with a local Maxwellian or with a slowing down distribution function. Considering the NEMO/SPOT distribution was numerically challenging in the full nonlinear GENE turbulence simulations. An increased number of markers is most likely required in NEMO/SPOT simulations in order to obtain a smoother numerical distribution compared to the coarse function with 4191 test particles used in this paper. However, as shown in the previous paragraph, no significant difference is expected by employing the numerical distribution function for the NBI fast deuterium. The values of the fluxes are computed as a time-average over the saturated state of the simulations. In Fig. 7 the time trace of the main ion and electron fluxes obtained with slowing down NBI fast deuterium and numerical TORIC/SSFPQL helium is shown with the corresponding average value used for Fig. 6. A significantly better agreement between numerical and experimental results is achieved with the more realistic distribution functions for the fast ion population. The experimental results are well reproduced by GENE simulations inside the temperature gradient error bars with both analytical (slowing down, bi-Maxwellian) and numerical (SSFPQL/TORIC-SELFO) distribution functions. In line with the linear results, a corresponding "weakening" of the (still significant) fast ion stabilisation is observed and, for the range of parameters here exploited, the bi-Maxwellian distribution is confirmed to be a good first order approximation to the more realistic backgrounds. Furthermore, a good agreement between GENE simulations based on TORIC and SELFO is here confirmed by the nonlinear results. The impact of the different fast ion distribution functions on the nonlinear transport levels can be further investigated through the study of the zonal flow structure. It has been shown in several publications[29–31] that zonal flows - as major nonlinear saturation mechanisms - can play a significant role in the reduction of turbulent fluxes. In gyrokinetic simulations, zonal flow activity is often measured through the $E \times B$ shearing rate defined as follows

$$\omega_{\mathrm{ZF}} = \frac{d^2\phi_{\mathrm{zon}}}{d^2x}. \tag{29}$$

Here, ϕ_{zon} is the zonal component of the electrostatic potential. In Fig. 8, the ratio between ω_{ZF}, averaged over all the k_x mode components, and the linear growth rate at the k_y of the transport flux maximum is shown for different values of the main ion temperature gradients and for the different fast ion distribution functions used in the nonlinear analysis of Fig. 6. A qualitative though correlation between $< \omega_{\mathrm{ZF}} >_{k_x} /\gamma_{\mathrm{lin}}$ and the turbulent flux levels is observed in Fig. 8. The zonal flow activity increases with a decrease of the main ion temperature gradients and lower fluxes are observed in GENE numerical simulations. These results suggest that the zonal flows are also affected by the more realistic fast-ion distribution functions and they are overestimated in the case of equivalent Maxwellian distributed fast ions. A more quantitative analysis will be done in future.

IV. CONCLUSIONS

In the present paper the collisionless δf gyrokinetic Vlasov-Maxwell coupled equations are re-derived for a completely arbitrary background distribution function in the full electromagnetic case. As a meaningful example for a possible application, a previous study on a

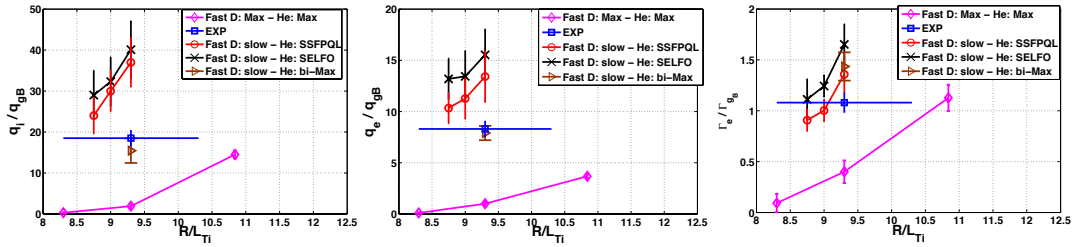

FIG. 6. Time-averaged nonlinear (a) main ion, (b) electron heat and (c) particle flux in GyroBohm units for different main ion temperature gradients and fast ion distribution functions.

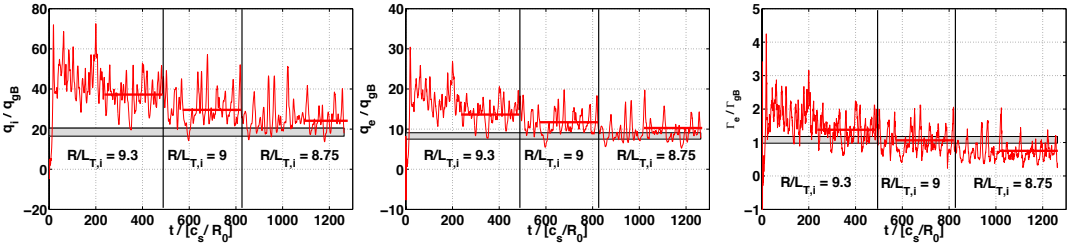

FIG. 7. Time trace of the nonlinear (a) main ion, (b) electron heat and (c) particle flux in GyroBohm units for different main ion temperature gradients for the case: slowing down fast deuterium and TORIC/SSFPQL fast helium. The gray area denotes the experimental value within error bars.

particular low beta JET plasma with significant fast ion stabilisation is revised with more realistic distribution functions for the fast ion population compared to the results obtained with equivalent Maxwellian background distributions. The bulk plasma is composed by Deuterium, electron and Carbon impurities, while the fast particles are NBI fast deuterium and ICRH accelerated ^{3}He. Electromagnetic effects, collisions and experimental geometry are taken into account in the simulations. In the linear analysis it is found that with the more realistic distribution functions the fast ion stabilisation still holds, even if it is weakened. This is in line with the previous nonlinear findings where gradients higher than the nominal ones had to be employed in order to match the experimental heat fluxes in the presence of fast particles[22]. The impact of the different non-Maxwellian backgrounds is studied separately on each fast ion species and a lack of sensitivity to the NBI fast ion distribution is observed. Generally, the choice of the ^{3}He background distribution - particular, its anisotropies and asymmetries - has a stronger impact on the linear results than the fast deuterium backgrounds. As discussed in this paper, a change in the background distribution affects the resonant ITG-fast ion stabilisation which, for this JET discharge, is particularly strong only for the fast helium population. These linear results are confirmed by GENE nonlinear turbulence simulations. An improved agreement between the experimental and numerical results is achieved for the main ion and electron fluxes at the nominal plasma parameters when more realistic fast-ion distribution functions are employed. Additionally, for the range of parameters considered here, the bi-Maxwellian and the slowing down distributions are shown to be good first order approximations for the fast helium and deuterium numerical backgrounds. A good agree-

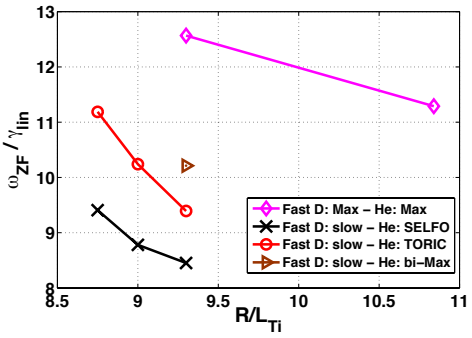

FIG. 8. Time-k_x averaged $E \times B$ shearing rate normalised to the linear growth rate at the k_y of the transport flux maximum for different main ion temperature gradients and for different fast ion distributions.

ment between nonlinear GENE results obtained using TORIC/SSFPQL and SELFO distribution functions is here confirmed. First results suggest that the choice of the background distribution function has also an impact on the level of zonal-flow activity.

ACKNOWLEDGEMENT

The simulations presented in this work were performed using the HYDRA cluster at the Rechenzentrum Garching (RZG), Germany. Furthermore, we acknowledge the CINECA award under the ISCRA initiative, for the availability of high performance computing resources and support. This work has been carried out within the framework of the EUROfusion Consortium and has received funding from the Euratom research and training programme 2014-2018 under grant agreement No 633053. The views and opinions expressed herein do not necessarily reflect those of the European Commission. The author would like to thank F. Jenko, Ph. Lauber and M. Romanelli for all the stimulating discussions, useful suggestions and comments.

REFERENCES

[1] F. Romanelli, Phys. Fluids B: Plasma Phys. **1**, 1018 (1989).
[2] G. Tardini, J. Hobirk, V. G. Igochine, C. F. Maggi, P. Martin, D. McCune, A. G. Peeters, A. C. C. Sips, A. Stäbler, J. Stober, and ASDEX Upgrade Team, Nucl. Fusion **47**, 280 (2007).
[3] C. Holland, C. C. Petty, L. Schmitz, K. H. Burrell, G. R. McKee, T. L. Rhodes, and J. Candy, Nucl. Fusion **52**, 114007 (2012).
[4] C. Bourdelle, G. T. Hoang, X. Litaudon, C. M. Roach, and T. Tala, Nucl. Fusion **45**, 110 (2005).
[5] M. Romanelli, A. Zocco, F. Crisanti, and JET Contributors, Plasma Phys. Controlled Fusion **52**, 045007 (2010).
[6] J. Citrin, J. Garcia, T. Görler, F. Jenko, P. Mantica, D. Told, C. Bourdelle, D. R. Hatch, G. M. D. Hogeweij, T. Johnson, M. J. Pueschel, and M. Schneider, Plasma Phys. Controlled Fusion **57**, 014032 (2015).
[7] A. Di Siena, T. Görler, H. Doerk, and E. Poli, Nucl. Fusion Lett. **58** (2018), 10.1088/1741-4326/aaaf26.
[8] G. J. Wilkie, I. Pusztai, I. Abel, W. Dorland, and T. Fülop, Plasma Phys. Controlled Fusion **59** (2017), 10.1088/1361-6587/aa5902.
[9] G. J. Wilkie, I. Abel, M. Landreman, and W. Dorland, Phys. Plasmas **23** (2016), 10.1063/1.4953420.
[10] M. Schneider, L. G. Eriksson, I. Jenkins, J. F. Artaud, V. Basiuk, F. Imbeaux, T. Oikawa, JET-EFDA contributors, and ITM-TF contributors, Nucl. Fusion **51**, 063019 (2011).
[11] J. Hedin, T. Hellsten, L. G. Eriksson, and T. Johnson, Nucl. Fusion **42**, 527 (2002).
[12] M. Brambilla, Nucl. Fusion **34**, 1121 (1994).
[13] M. Brambilla, Plasma Phys. Controlled Fusion **31**, 723 (1989).
[14] F. Jenko, W. Dorland, M. Kotschenreuther, and B. N. Rogers, Phys. Plasmas **7**, 1904 (2000).
[15] T. Görler, X. Lapillonne, S. Brunner, T. Dannert, F. Jenko, F. Merz, and D. Told, Journal of Computational Physics **230**, 7053 (2011).
[16] P. Xanthopoulos, H. E. Mynick, P. Helander, Y. Turkin, G. G. Plunk, F. Jenko, T. Görler, D. Told, T. Bird, and H. J. E. Proll, Phys. Rev. Lett. **113**, 155001 (2014).
[17] A. J. Brizard and T. S. Hahm, Rev. Mod. Phys. **79**, 421 (2007).
[18] T. Dannert, S. Günter, T. Hauff, F. Jenko, X. Lapillonne, and P. Lauber, Phys. Plasmas **15**, 062508 (2008).
[19] A. Di Siena, T. Görler, H. Doerk, J. Citrin, T. Johnson, M. Schneider, E. Poli, and JET Contributors, J. Phys. Conf. Ser. **775**, 012003 (2016).
[20] P. Mantica, D. Strintzi, T. Tala, C. Giroud, T. Johnson, H. Leggate, E. Lerche, T. Loarer, A. G. Peeters,

A. Salmi, S. Sharapov, D. Van Eester, P. C. de Vries, L. Zabeo, and K.-D. Zastrow, Phys. Rev. Lett. **102**, 175002 (2009).
[21] P. Mantica, C. Angioni, C. Challis, G. Colyer, L. Frassinetti, N. Hawkes, T. Johnson, M. Tsalas, P. C. de Vries, J. Weiland, B. Baiocchi, M. N. A. Beurskens, A. C. A. Figueiredo, C. Giroud, J. Hobirk, E. Joffrin, E. Lerche, V. Naulin, A. G. Peeters, A. Salmi, C. Sozzi, D. Strintzi, G. Staebler, T. Tala, D. Van Eester, and T. Versloot, Phys. Rev. Lett. **107**, 135004 (2011).
[22] J. Citrin, F. Jenko, P. Mantica, D. Told, C. Bourdelle, J. Garcia, J. W. Haverkort, G. M. D. Hogeweij, T. Johnson, and M. J. Pueschel, Phys. Rev. Lett. **111**, 155001 (2013).
[23] R. Bravenec, J. Citrin, J. Candy, P. Mantica, T. Görler, and JET Contributors, Plasma Phys. Controlled Fusion **58** (2016), 10.1088/0741-3335/58/12/125018.
[24] J. D. J. Gaffey, J. Plasma Phys. **16**, 149 (1976).
[25] C. Angioni and A. G. Peeters, Phys. Plasmas **15**, 052307 (2008).
[26] C. Estrada-Mila, J. Candy, and R. E. Waltz, Phys. Plasmas **13**, 112303 (2006).
[27] J. Citrin, F. Jenko, P. Mantica, D. Told, C. Bourdelle, R. Dumont, J. Garcia, J. W. Haverkort, G. M. D. Hogeweij, T. Johnson, M. J. Pueschel, and JET-EFDA contributors, Nucl. Fusion **54**, 023008 (2014).
[28] J. F. Artaud, Nucl. Fusion **50**, 043001 (2010).
[29] F. Jenko and A. Kendl, Phys. Plasmas **9**, 4103 (2002).
[30] P. H. Diamond, S. I. Itoh, K. Itoh, and T. S. Hahm, Plasma Phys. Controlled Fusion **47** (2005), 10.1088/0741-3335/47/5/R01.
[31] M. J. Pueschel, D. R. Hatch, T. Görler, W. M. Nevins, F. Jenko, P. W. Terry, and D. Told, Phys. Plasmas **20**, 102301 (2013).